Additive Noise and Jitter Performance Analysis of Passive Optical Interferometers Operated at Ultrahigh Rates

Konstantinos Yiannopoulos, George Theodore Kanellos, Nikos Pleros, and Hercules Avramopoulos

***Abstract*—In this paper, we theoretically associate the additive noise, the amplitude jitter and the timing jitter at the input and output of passive optical interferometers. We make use of the theoretical results to assess the noise and jitter performance of interferometer based applications such as pulse repetition frequency multiplication and clock recovery. We show that, for both applications, interferometers may successfully reduce the noise and the jitter existing in the input signals, and thus yield very high quality output signals. Furthermore, we focus on the practical aspects of deploying Fabry–Pérot interferometers in rate multipliers and clock recoveries, and provide rules for selecting the characteristics of the Fabry–Pérot interferometer to meet specific quality requirements for the output signal.**

***Index Terms*—Additive noise, amplitude jitter, clock recovery, Fabry–Pérot interferometers, interferometers, optical signal processing, pulse repetition frequency multiplication, timing jitter.**

I. Introduction

PASSIVE interferometers appear to be well-suited candidates for deployment in optical signal generation and signal recovery applications, including high rate optical sources [1]–[4], burst generators [5], [6], coders/decoders [7], [8], clock recoveries [9]–[13], and receivers [14]. This mainly owes to their characteristic impulse response that can be properly tailored to meet specific performance requirements in each respective application, as well as to their capability of performing in ultrahigh bit rates exceeding hundreds of gigabits per second. However, operating optical subsystems employing passive interferometers at ultrahigh rates imposes severe limitations regarding the measurements that have to be performed upon the pulse train at the output of the interferometer. In particular, amplitude and timing jitter of the output pulse train are key parameters when assessing the output signal quality but can not be easily measured due to the limitations in the test equipment. So far, several methods have been proposed for calculating the amplitude and timing jitter of ultrahigh-rate pulse trains, including radio frequency spectrum analysis [15], [16], intermediate frequency spectrum analysis after electrical frequency down-conversion [17], time-domain demodulation after optical down-conversion [18] and optical cross correlation [19].

In the present work, we propose a novel theoretical method for estimating the amplitude and timing jitter at the output of interferometer based systems. This method relies on the association of the amplitude and timing jitter at the input and output of the interferometer in terms of its impulse response, or equivalently its transfer function. As a result, the root-mean-square values of the amplitude and timing jitter at the output of the interferometer are expressed as a function of the interferometer impulse response and their respective values at the input. We apply this method to split-and-delay and to Fabry–Pérot interferometric configurations performing rate multiplication, showing that the infinite duration of the impulse response of the Fabry–Pérot makes it possible to reduce the input jitter, while the split-and-delay interferometers (SDIs) suffer from excessive timing jitter. Moreover, we discuss the interferometer based clock recovery scheme and examine the applicability of Fabry–Pérot interferometers as retiming elements, revealing that the Fabry–Pérots successfully retime the incoming data by reducing the timing jitter below 50% for pseudo-random bit sequences (PRBS), making them perfectly suitable for deployment in 3R regenerative setups. As such, the proposed method provides accurate estimation for amplitude and timing jitter for systems operating at over multihundred of gigabits per second, where the direct measurement of both quantities is not feasible, as well as a valid estimate for lower rate systems, where the amplitude and timing jitter measurement precision is limited, as for example when the jitter is estimated by suppressed radio frequency (RF) harmonics [1], or only a couple of RF harmonics is available [15]. Finally, this method can be applied to design optimal applications of interferometers minimizing amplitude and timing jitter of the output signal.

The rest of the paper is divided into three sections. In Section II, we make a detailed discussion on the response of the interferometer when driven by a nondeterministic signal, as is the case of jitter, and we derive the equations that associate the input and output jitter. To this end, Section II includes the impact of the interferometer response on additive noise and provides a noise figure (NF) calculation, as well. In Section III we apply the results of the theory on the rate multiplication technique and assess the noise and jitter performance of split-and-delay and Fabry–Pérot interferometers performing rate multiplication. Finally, in Section IV we discuss the interferometer-based clock recovery scheme and examine the applicability of Fabry–Pérot interferometers as retiming elements.

Manuscript received February 14, 2006; revised May 30, 2006.

K. Yiannopoulos was with the School of Electrical and Computer Engineering, National Technical University of Athens, Zografou 15773, Greece. He is now with the Department of Computer Engineering and Informatics, University of Patras, Patras 26500, Greece (e-mail: giannopu@ceid.upatras.gr).

G. T. Kanellos, N. Pleros, and H. Avramopoulos are with the School of Electrical and Computer Engineering, National Technical University of Athens, Zografou 15773, Greece (e-mail: gkanel@mail.ntua.gr; pleros@mail.ntua.gr; hav@cc.ece.ntua.gr).

Digital Object Identifier 10.1109/JQE.2006.880070

II. Theoretical Analysis

The aim of this section is to associate the amplitude and timing root-mean-square (rms) jitter deviation, as well as the additive noise power at the input and output of the passive optical interferometer. We begin our analysis considering that the input optical signal suffers from amplitude $A(t)$ and timing $J(t)$ jitter, which lie in the small signal domain $(A(t), J(t) \ll 1)$. As a result, the optical power may be written as [15], [20]

$$P_X(t) = P(t) + A(t) \cdot P(t) - T \cdot J(t) \cdot \dot{P}(t) \tag{1}$$

where $P(t)$ is the power of the perfect (jitter-free) signal, $\dot{P}(t)$ is the time derivative of the signal power, and T is the bit period of the signal. Although it is common practice to measure the jitter in the optical power domain of (1) [15], [20], [21], we need to find the respective optical field, since the optical interferometer impulse response we use later on in this section is valid only for optical fields. Under the small signal assumption for the jitter, we can express the optical field as

$$X(t) = \sqrt{P_X(t)} \cong E(t) + \frac{A(t)}{2} \cdot E(t) - T \cdot J(t) \cdot \dot{E}(t). \tag{2}$$

Based on (1) and (2) the rms amplitude and timing jitter deviations as measured in the field domain σ_A^E, σ_J^E and the rms amplitude and timing jitter deviations as measured in the power domain σ_A^P, σ_J^P are related as follows:

$$\sigma_A^P = 2 \cdot \sigma_A^E \tag{3}$$

$$\sigma_J^P = \sigma_J^E \tag{4}$$

Thus, although we will refer to the field rms jitter deviation for the rest of the paper, unlike the commonly used power rms jitter deviation, the association between them is straightforward.

After including the additive noise term in (2), we finally obtain the signal at the input of the interferometer

$$X(t) = E(t) + N(t) + \frac{A(t)}{2} \cdot E(t) - T \cdot J(t) \cdot \dot{E}(t). \tag{5}$$

The next step is to calculate the rms jitter deviation and noise power of the input signal, by means of the autocorrelation function of $X(t)$. Under the conditions that $A(t)$, $J(t)$, and $N(t)$ are zero mean, wide-sense stationary stochastic processes, the autocorrelation function is given by

$$R_X(\tau) = R_E(\tau) + R_N(\tau) + \frac{R_A(\tau)}{4} \cdot R_E(\tau) + T^2 \cdot R_J(\tau) \cdot \ddot{R}_E(\tau) \tag{6}$$

The input signal signal-to-noise ratio (SNR) and jitter rms deviations are then calculated by

$$\mathrm{SNR} = \frac{R_{XE}(0)}{R_{XN}(0)} = \frac{R_E(0)}{R_N(0)} \tag{7}$$

$$\sigma_A^2 = \frac{R_{XA}(0)}{R_{XE}(0)} = \frac{R_A(0)}{4} \tag{8}$$

$$\sigma_J^2 = \frac{R_{XJ}(0)}{R_{X\dot{E}}(0)} = R_J(0). \tag{9}$$

In (7)–(9) $R_{XZ}(\tau)$, $Z = E, A, J, N$ denote the contribution of the optical field, amplitude jitter, timing jitter and additive noise autocorrelations, respectively, to the input autocorrelation function.

In as similar fashion, we need to evaluate the autocorrelation function $R_Y(\tau)$ of the stochastic process $Y(t)$ at the output of the interferometer, and then calculate the SNR and rms output jitter deviations. The autocorrelation function of the signal at the output is given by

$$R_Y(\tau) = \int_{-\infty}^{\infty}\int h(\tau_1) \cdot h^*(\tau_2) \cdot R_X(\tau - \tau_1 + \tau_2) \cdot d\tau_1 \cdot d\tau_2 \tag{10}$$

where $h(t)$ is the impulse response function of the interferometer

$$h(t) = \sum_{i=0}^{\infty} h_i \cdot \delta\left(t - \frac{i}{\mathrm{FSR}}\right). \tag{11}$$

We evaluate the integral of (10) and we find that

$$R_Y(\tau) = \sum_{k=-\infty}^{\infty} C_k \cdot R_X\left(\tau - \frac{k}{\mathrm{FSR}}\right). \tag{12}$$

In (12) we have introduced the discrete autocorrelation coefficients C_k of the interferometer, calculated by

$$C_k = \sum_{i=0}^{\infty} h_i \cdot h_{i+k}^*. \tag{13}$$

The SNR and rms jitter deviations at the output are given by

$$\mathrm{SNR} = \frac{R_{YE}(0)}{R_{YN}(0)} = \frac{\sum_{k=-\infty}^{\infty} C_k \cdot R_E\left(\frac{k}{\mathrm{FSR}}\right)}{\sum_{k=-\infty}^{\infty} C_k \cdot R_N\left(\frac{k}{\mathrm{FSR}}\right)} \tag{14}$$

$$\sigma_A^2 = \frac{R_{YA}(0)}{R_{YE}(0)} = \frac{\sum_{k=-\infty}^{\infty} C_k \cdot R_A\left(\frac{k}{\mathrm{FSR}}\right) \cdot R_E\left(\frac{k}{\mathrm{FSR}}\right)}{4 \cdot \sum_{k=-\infty}^{\infty} C_k \cdot R_E\left(\frac{k}{\mathrm{FSR}}\right)} \tag{15}$$

$$\sigma_J^2 = \frac{R_{YJ}(0)}{R_{Y\dot{E}}(0)} = \frac{\sum_{k=-\infty}^{\infty} C_k \cdot R_J\left(\frac{k}{\mathrm{FSR}}\right) \cdot \ddot{R}_E\left(\frac{k}{\mathrm{FSR}}\right)}{\sum_{k=-\infty}^{\infty} C_k \cdot \ddot{R}_E\left(\frac{k}{\mathrm{FSR}}\right)}. \tag{16}$$

The autocorrelation contributions $R_{YZ}(\tau)$ in (14)–(16) are defined similar to the contributions to the input signal autocorrelation $R_X(\tau)$.

In order to simplify (14)–(16) we need to evaluate the autocorrelation function $R_E(\tau)$ of the jitter-free optical signal. We assume that the optical signal is in return-to-zero format with a bit period equal to $T = \mathrm{FSR}^{-1}$, thus it may be written as

$$E(t) = \sum_i a_i \cdot g(t + i \cdot T) \tag{17}$$

where $g(t)$ is the function that describes the optical pulse and $a_i = \{0, 1\}$ indicates the data signal encoded on the respective pulse. The autocorrelation function of the optical signal is then given by [22]

$$R_E(\tau) = \frac{1}{T} \cdot \sum_k A_k \cdot R_g(\tau + k \cdot T) \tag{18}$$

where $R_g(\tau)$ is the autocorrelation function of the optical pulse and A_k is the discrete autocorrelation function of the data, calculated by

$$A_k = E\left\{a_i \cdot a_{i+k}^*\right\}. \tag{19}$$

From (18) we see that if the optical pulse duration is short with respect to the bit period, which is the case in return-to-zero formats, then there is no interference between successive pulses at the autocorrelation function, thus

$$R_E\left(\frac{k}{\mathrm{FSR}}\right) = \frac{1}{T} \cdot A_k \cdot R_g(0). \tag{20}$$

After replacing the autocorrelation function in (14)–(16), they simplify to

$$\mathrm{SNR} = \frac{R_g(0) \cdot \sum\limits_{k=-\infty}^{\infty} C_k \cdot A_k}{T \cdot \sum\limits_{k=-\infty}^{\infty} C_k \cdot R_N\left(\frac{k}{\mathrm{FSR}}\right)} \tag{21}$$

$$\sigma_A^2 = \frac{\sum\limits_{k=-\infty}^{\infty} C_k \cdot A_k \cdot R_A\left(\frac{k}{\mathrm{FSR}}\right)}{4 \cdot \sum\limits_{k=-\infty}^{\infty} C_k \cdot A_k} \tag{22}$$

$$\sigma_J^2 = \frac{\sum\limits_{k=-\infty}^{\infty} C_k \cdot A_k \cdot R_J\left(\frac{k}{\mathrm{FSR}}\right)}{\sum\limits_{k=-\infty}^{\infty} C_k \cdot A_k}. \tag{23}$$

The last step of the theoretical analysis is to associate the rms jitter deviations and SNRs at the output and input of the interferometer. We make this association after defining the NF and rms jitter deviation ratios

$$\mathrm{NF} = \frac{\mathrm{SNR}_{\mathrm{out}}}{\mathrm{SNR}_{\mathrm{in}}} \tag{24}$$

$$\rho_A = \frac{\sigma_{A,\mathrm{out}}}{\sigma_{A,\mathrm{in}}} \tag{25}$$

$$\rho_J = \frac{\sigma_{J,\mathrm{out}}}{\sigma_{J,\mathrm{in}}}. \tag{26}$$

After combining (7)–(9) and (21)–(23) we finally obtain

$$\mathrm{NF} = \frac{\sum\limits_{k=-\infty}^{\infty} C_k \cdot A_k}{A_0 \cdot \sum\limits_{k=-\infty}^{\infty} C_k \cdot r_N\left(\frac{k}{\mathrm{FSR}}\right)} \tag{27}$$

$$\rho_{A,J} = \sqrt{\frac{\sum\limits_{k=-\infty}^{\infty} C_k \cdot A_k \cdot r_{A,J}\left(\frac{k}{\mathrm{FSR}}\right)}{\sum\limits_{k=-\infty}^{\infty} C_k \cdot A_k}} \tag{28}$$

where

$$r_{N,A,J}(\tau) = \frac{R_{N,A,J}(\tau)}{R_{N,A,J}(0)} = \frac{\int_{-\infty}^{\infty} S_{N,A,J}(f) \cdot e^{j2\pi f\tau} \cdot df}{\int_{-\infty}^{\infty} S_{N,A,J}(f) \cdot df} \tag{29}$$

denotes the respective normalized noise or jitter autocorrelation function.

We conclude this section by commenting on several assumptions we have made. A key assumption is that jitter and noise are wide sense stationary processes, therefore their autocorrelation functions depend only on variable τ. However, when the jitter and noise processes are nonstationary, their autocorrelation functions must be replaced by $R_Z(t, \tau)$, and as a result, the respective rms deviations will vary with time. Filtering nonstationary processes is possible by deploying adaptive filters [23], but this is beyond the scope of this paper. A second assumption is that the amplitude jitter $A(t)$ is uncorrelated with the optical field $E(t)$. Our analysis is still valid in a more realistic scenario, in which the amplitude jitter and the optical field are correlated. In such case, the products of the individual autocorrelation functions of the optical field $R_E(\tau)$ and the amplitude jitter $R_A(\tau)$ are replaced by the cross correlation function $R_{EA}(\tau)$ in (8) and (15). Finally, we have neglected the effect of interferometric phase noise, assuming that the coherence time of the optical field is much larger than the bit period. Despite the fact that this is not true in most optical systems, the coherence time of the optical field can be increased in an incoherent-to-coherent wavelength converter [24] deployed at the input of the interferometer [25].

In the following sections, we apply (27) and (28) to evaluate the performance of interferometer-based rate multipliers and clock recoveries.

III. Rate Multiplication

The rate multiplication technique has been extensively studied by several research groups, since it is capable of producing ultrahigh rate pulse trains in a simple and robust fashion. In rate multiplication, a high free spectral range (FSR)

interferometer is triggered by a low-rate optical signal with period equal to T_{in}, and as a consequence the rate of the optical signal is multiplied by a factor equal to $m = T_{\text{in}} \cdot \text{FSR}$. The low rate signal may be viewed upon as a repetitive pattern of one "1" followed by $m-1$ "0's," thus the period of the input signal relates to the bit period as $T_{\text{in}} = m \cdot T$. This approach is consistent with the notation of the a coefficients of (17), which are given by

$$a_i = \begin{cases} 1, & (i = j \cdot m) \\ 0, & (i \neq j \cdot m) \end{cases} \tag{30}$$

while the respective discrete autocorrelation function is calculated as

$$A_k = \begin{cases} \frac{1}{m} & (k = j \cdot m) \\ 0 & (k \neq j \cdot m). \end{cases} \tag{31}$$

We introduce (31) into (27) and (28) to study the noise and jitter performance of the interferometers.

A. Noise Figure (NF) Analysis

After combining (27) and (31) we obtain

$$\text{NF} = \frac{\sum\limits_{j=-\infty}^{\infty} C_{j \cdot m}}{\sum\limits_{j=-\infty}^{\infty} C_j \cdot r_N\left(\frac{j}{\text{FSR}}\right)} \tag{32}$$

which shows that the NF of the rate multiplication process depends only on the interferometer correlation function and the noise spectral power density $S_N(f)$. Since in most practical cases the additive noise spectral bandwidth Δf is much larger than the interferometer FSR, the noise autocorrelation function is a delta function. Thus, (32) simplifies to

$$\text{NF} = \frac{\sum\limits_{j=-\infty}^{\infty} C_{j \cdot m}}{C_0}. \tag{33}$$

To further elaborate in the study of noise performance in rate multiplication we study two commonly deployed types of interferometers, the SDI and the Fabry–Pérot filter (FPF). The SDI produces m successive equal amplitude replicas of a single pulse, thus its transfer function is given by

$$h^{\text{SDI}}(t) = \frac{1}{m} \cdot \sum_{i=0}^{m-1} \delta\left(t - \frac{i}{\text{FSR}}\right) \tag{34}$$

The respective discrete autocorrelation function of the interferometer is calculated as

$$C_k^{\text{SDI}} = \begin{cases} \frac{1}{m} \cdot \left(1 - \frac{|k|}{m}\right) & (|k| < m) \\ 0 & (|k| \geq m). \end{cases} \tag{35}$$

After combining (33) and (35) we find that the NF is given by

$$\text{NF}^{\text{SDI}} = \frac{C_0^{\text{SDI}}}{C_0^{\text{SDI}}} = 1. \tag{36}$$

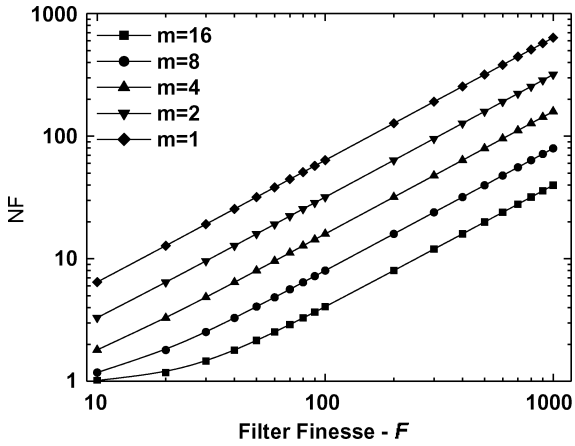

Fig. 1. Rate multiplication with the FPF: calculated NF versus the FPF finesse for multiplication factors $m = 1, \ldots, 16$.

Thus, SDI-based rate multipliers are capable of performing rate multiplication without altering the NF of the input signal.

This is not the case however in FPF-based multipliers. The FPF does not produce equal amplitude replicas of a single pulse, but its impulse response function is exponentially decaying. Since their impulse response function lasts for over m pulses, FPFs suffer from pulse to pulse amplitude variations which may significantly degrade the output signal if not dealt with [1], [2]. However, the fact that the duration of the FPFs impulse response is over m pulses gives them the advantage of better filtering the noise, thus enhancing the NF. In order to assess the noise and jitter performance of the FPFs we first calculate their discrete autocorrelation function

$$C_k^{\text{FPF}} = \frac{1-R}{1+R} \cdot R^{|k|} \tag{37}$$

where R is the FPF mirror reflectivity. By combining (33) and (37) we calculate the NF

$$\text{NF}^{\text{FPF}} = \sum_{j=-\infty}^{\infty} R^{|j| \cdot m} = \frac{1+R^m}{1-R^m}. \tag{38}$$

The NF of (38) is plotted in Fig. 1 against the FPF finesse for multiplication factors $m = 1, \ldots, 16$. As it can be verified from Fig. 1 rate multiplication in the FPF achieves very high NFs, and after curve fitting we find that the NF can be approximated by

$$\text{NF}^{\text{FPF}} = \frac{0.63 \cdot F}{m} \tag{39}$$

which provides a rule of the thumb for selecting the finesse of the FPF in the rate multiplier when noise performance enhancement is required, and this might be the case if the low rate signal introduced to the FPF is of poor quality. In such case, the respective SDI-based multiplier would maintain the poor quality of the signal.

B. Amplitude and Timing Jitter Analysis

As far as the amplitude jitter is concerned we combine (28) and (31) to obtain

$$\rho_A = \sqrt{\frac{\sum_{j=-\infty}^{\infty} C_{j\cdot m} \cdot r_A\left(\frac{j\cdot m}{\mathrm{FSR}}\right)}{\sum_{j=-\infty}^{\infty} C_{j\cdot m}}} \tag{40}$$

$$\rho_J = m \cdot \sqrt{\frac{\sum_{j=-\infty}^{\infty} C_{j\cdot m} \cdot r_J\left(\frac{j\cdot m}{\mathrm{FSR}}\right)}{\sum_{j=-\infty}^{\infty} C_{j\cdot m}}}. \tag{41}$$

The multiplication factor m is introduced in (41) so as to relate the output timing jitter deviation with the resulting repetition period, since $T_{\mathrm{in}} = m \cdot T_{\mathrm{out}}$.

We use (40) and (41) to study the jitter performance of SDI- and FPF-based rate multipliers. As far as the SDIs are concerned, we make use of their autocorrelation function to obtain

$$\rho_A^{\mathrm{SDI}} = \sqrt{\frac{C_0^{\mathrm{SDI}} \cdot r_A(0)}{C_0^{\mathrm{SDI}}}} = 1 \tag{42}$$

$$\rho_J^{\mathrm{SDI}} = m \cdot \sqrt{\frac{C_0^{\mathrm{SDI}} \cdot r_J(0)}{C_0^{\mathrm{SDI}}}} = m. \tag{43}$$

As a result, SDI rate multipliers leave amplitude jitter unaffected, but drastically degrade the timing jitter. Thus, SDI-based rate multipliers require low rate triggering pulse trains of very high fidelity. The fidelity requirements may be relaxed, however, in FPF-based rate multipliers. When FPFs are employed, the jitter rms deviation ratios become

$$\rho_A^{\mathrm{FPF}} = \sqrt{\frac{\sum_{j=-\infty}^{\infty} R^{|j|\cdot m} \cdot r_A\left(\frac{j\cdot m}{\mathrm{FSR}}\right)}{\sum_{j=-\infty}^{\infty} R^{|j|\cdot m}}} = \sqrt{\frac{1-R^m}{1+R^m} \cdot \sum_{j=-\infty}^{\infty} R^{|j|\cdot m} \cdot r_A\left(\frac{j\cdot m}{\mathrm{FSR}}\right)} \tag{44}$$

$$\rho_J^{\mathrm{FPF}} = m \cdot \sqrt{\frac{1-R^m}{1+R^m} \cdot \sum_{j=-\infty}^{\infty} R^{|j|\cdot m} \cdot r_J\left(\frac{j\cdot m}{\mathrm{FSR}}\right)} \tag{45}$$

Equations (44) and (45) are plotted versus the FPF finesse and for several multiplication factors in Fig. 2. The graphs have been plotted considering a Gaussian jitter spectral power density

$$S_{A,J}(f) = \exp\left(-\frac{f}{\Delta f}\right)^2. \tag{46}$$

Depending on the bandwidth Δf of the jitter spectral power density $S_{A,J}(f)$, jitter is categorized as being correlated [16], [21] or uncorrelated [20], [21]. In the uncorrelated jitter regime, the jitter bandwidth is much larger than the interferometer FSR, thus the jitter autocorrelation function is practically a delta function, similar to the additive noise analysis case. Considering that the jitter is uncorrelated, (40) and (41) reduce to

$$\rho_{A,unc}^{\mathrm{FPF}} = \sqrt{\frac{C_0}{\sum_{j=-\infty}^{\infty} C_{j\cdot m}}} = \sqrt{\frac{1-R^m}{1+R^m}} \tag{47}$$

$$\rho_{J,unc}^{\mathrm{FPF}} = m \cdot \sqrt{\frac{C_0}{\sum_{j=-\infty}^{\infty} C_{j\cdot m}}} = m \cdot \sqrt{\frac{1-R^m}{1+R^m}} \tag{48}$$

which shows that it is possible to reduce uncorrelated timing jitter in an FPF-based rate multiplier only when

$$\frac{1+R^m}{1-R^m} > m^2 \tag{49}$$

and in such case the amplitude jitter ratio is also reduced to

$$\rho_{A,unc}^{\mathrm{FPF}} < \frac{1}{m}. \tag{50}$$

The uncorrelated amplitude and timing jitter rms deviation ratios are plotted in Fig. 2-1(a) and 2-2(a), respectively. As it can be verified from these figures, it is always possible to reduce amplitude jitter, however timing jitter may be reduced upon the condition described in (49), and higher FPF finesses are required as the multiplication factor increases.

Contrary to the uncorrelated jitter regime, in the correlated jitter regime the jitter bandwidth Δf is orders of magnitude smaller than the FPF FSR. In the extreme limit where the jitter bandwidth is infinitesimally small (fully correlated jitter) with respect to the FSR, the autocorrelation function $r_{A,J}(\tau)$ equals unity for all τ, and (44) and (45) reduce to

$$\rho_{A,\mathrm{cor}}^{\mathrm{FPF}} \cong 1 \tag{51}$$

$$\rho_{J,\mathrm{cor}}^{\mathrm{FPF}} \cong m. \tag{52}$$

Thus, the FPF, much like the SDI, is not capable of reducing the fully correlated amplitude jitter and aggravates the correlated timing jitter by the multiplication factor m, and this is clearly shown in Fig. 2-1(c) and 2-2(c). The results of (51) and (52) generally hold for any type of interferometer-based rate multiplier operating in the correlated jitter regime, and this can be shown after we replacing $r_{A,J}(\tau) = 1$ in (40) and (41).

Finally, when the jitter bandwidth is close to the FPF FSR (partially correlated jitter) [26], (44) and (45) cannot simplify and have to be calculated. The case of partially correlated jitter is shown in Fig. 2-1(b) and 2-2(b). Fig. 2-1(b) shows that, like the uncorrelated and fully correlated cases, it is always feasible to reduce the amplitude jitter, and the degree of reduction lies between the two extremes. Similarly, Fig. 2-1(b) shows that it is not always possible to reduce timing jitter, however when this is possible higher finesse values are required with respect to the uncorrelated jitter case.

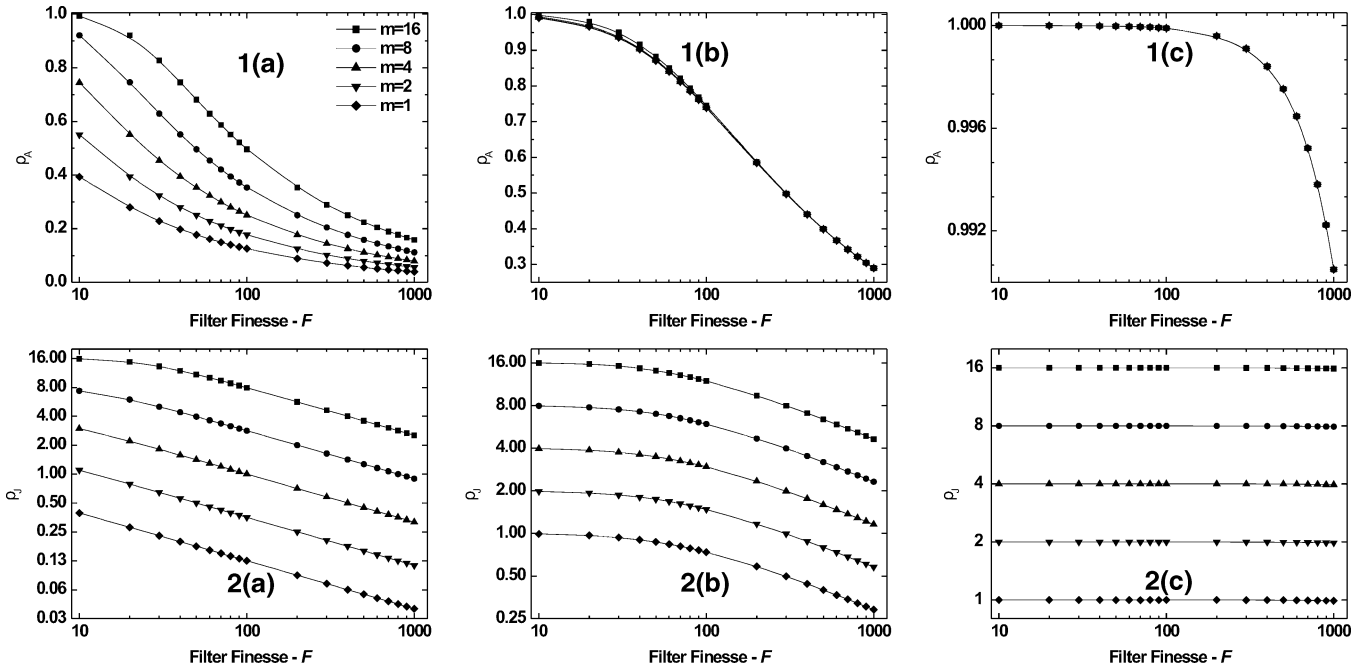

Fig. 2. Rate multiplication with the FPF: calculated amplitude and timing jitter ratios versus the FPF finesse for multiplication factors $m = 1, \ldots, 16$. $\Delta f/\mathrm{FSR}$ equals ∞, 10^{-2}, and 10^{-4} in columns (a), (b), and (c), respectively.

IV. Clock Recovery

Clock recovery is a crucial optical node functionality, for it provides the necessary synchronization in optical subsystems, such as optical receivers [14], 3R-regenerators [27], and header processing circuits [28]. Experimental results have shown that the timing and amplitude jitter of the recovered clock in interferometer-based clock recoveries is less than that of the incoming data [14], [29], and this has been taken advantage of in the experimental demonstration of an all-optical receiver [14]. In the current section, we confirm these experimental results.

In interferometer-based clock recovery, the interferometer FSR is chosen to be equal to the inverse of the bit period of the incoming signal, and as a result the interferometer isolates the spectral components of the signal that lie near multiples of the FSR, yielding a clock resembling signal at the output. In the time domain this process corresponds to partially filling the data pattern "0's" with "1's," and this random distribution of "0's" and "1's" in the a coefficients of (17) has to be taken into account when the NF and rms jitter deviation ratios of (27) and (28) are calculated. Although (27) and (28) are consistent for any type of the incoming data, we assume that the data form a PRBS of order n, the autocorrelation function of which is given by

$$A_k = \begin{cases} \dfrac{N+1}{2N} & (k = j \cdot N) \\ \dfrac{N+1}{4N} & (k \neq j \cdot N) \end{cases} \tag{53}$$

with $N = 2^n - 1$ being the PRBS period [30]. We introduce (53) in (27) and (28) to study the regenerative properties, with respect to the noise and jitter, of the interferometer-based clock recoveries.

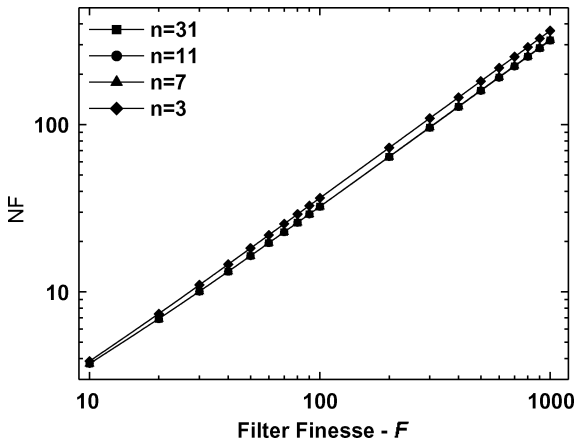

Fig. 3. Clock recovery with the FPF: calculated NF versus the FPF finesse for PRBS order $n = 3, 7, 11, 31$.

A. NF Analysis

We combine (27) and (53) to obtain

$$\mathrm{NF} = \frac{\sum_{j=-\infty}^{\infty} C_j + C_{j \cdot N}}{2 \cdot \sum_{j=-\infty}^{\infty} C_j \cdot r_N\left(\frac{j}{\mathrm{FSR}}\right)}. \tag{54}$$

If the additive noise bandwidth is large compared to the interferometer FSR (54) simplifies to

$$\mathrm{NF} = \frac{\sum_{j=-\infty}^{\infty} C_j + C_{j \cdot N}}{2 \cdot C_0}. \tag{55}$$

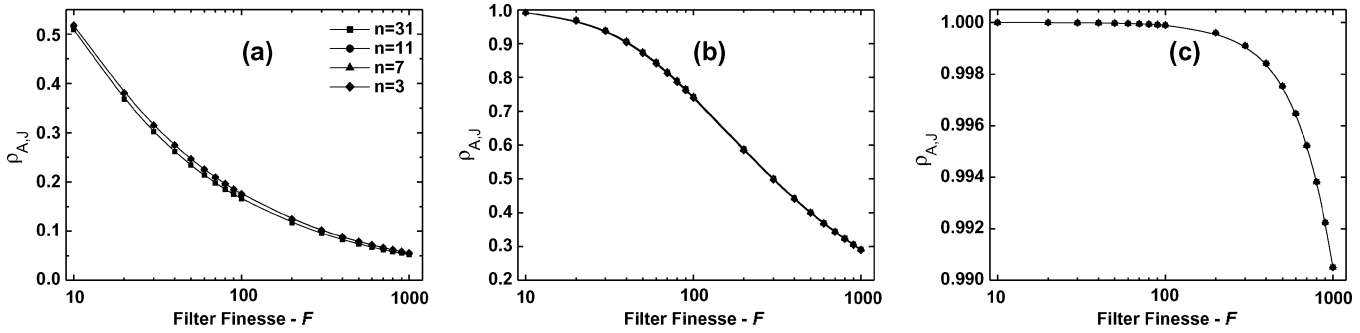

Fig. 4. Clock recovery with the FPF: calculated amplitude and timing jitter ratios versus the FPF finesse for PRBS order $n = 3, 7, 11, 31$. $\Delta f/\mathrm{FSR}$ equals ∞, 10^{-2}, and 10^{-4} in columns (a), (b), and (c), respectively.

This shows in a straightforward manner that the NF is always enhanced in interferometer-based clock recoveries, and this is to be expected, since the interferometer rejects the additive noise that does not lie near the clock harmonics. For a quantitive analysis of (55) we consider the case when the clock recovery is performed in a FPF, for which case the NF is calculated as

$$\mathrm{NF}^{\mathrm{FPF}} = \frac{1}{2} \cdot \left(\frac{1+R}{1-R} + \frac{1+R^N}{1-R^N} \right) \tag{56}$$

which is plotted in Fig. 3 versus the FPF finesse for PRBS orders $n = 3, 7, 11, 31$. Fig. 3 shows that clock recovery in the FPF achieves very high NFs which vary linearly with the FPF finesse, and as a rule of the thumb the NF is approximated by

$$\mathrm{NF}^{\mathrm{FPF}} = 0.35 \cdot F. \tag{57}$$

Noise figure improvement is achieved irrespective of the PRBS order, and this is demonstrated in Fig. 3 where curves for $n = 7$, 11,31 overlap. This is so, since the PRBS period relates exponentially to the PRBS order, and as a result R^N is practically zero for all PRBS orders in (56).

B. Amplitude and Timing Jitter Analysis

In a similar fashion, we combine (28) and (53) to obtain the jitter rms deviation ratios

$$\rho_{A,J} = \sqrt{\frac{\sum\limits_{j=-\infty}^{\infty} C_{j\cdot N} \cdot r_{A,J}\left(\frac{j\cdot N}{\mathrm{FSR}}\right) + C_j \cdot r_{A,J}\left(\frac{j}{\mathrm{FSR}}\right)}{\sum\limits_{j=-\infty}^{\infty} C_{j\cdot N} + C_j}}. \tag{58}$$

This shows that both the amplitude and timing jitter of the generated clock signal is always reduced with respect to the jitter of the incoming data, and the degree of reduction depends strongly on the duration of the jitter autocorrelation function. If the data jitter varies between successive pulses then the jitter spectral power density bandwidth Δf is much larger than the interferometer FSR, similar to the uncorrelated jitter regime of the rate multiplication case. Consequently, the jitter autocorrelation function is practically a delta function and then the rms jitter deviation ratios simplify to

$$\rho_{A,J} = \sqrt{\frac{2 \cdot C_0}{\sum\limits_{j=-\infty}^{\infty} C_{j\cdot N} + C_j}}. \tag{59}$$

For the FPF-based clock recovery, (58) is written as

$$\rho_{A,J}^{\mathrm{FPF}} = \sqrt{\frac{\sum\limits_{j=-\infty}^{\infty} R^{|j|\cdot N} \cdot r_J\left(\frac{j\cdot N}{\mathrm{FSR}}\right) + R^{|j|} \cdot r_J\left(\frac{j}{\mathrm{FSR}}\right)}{\sum\limits_{j=-\infty}^{\infty} R^{|j|\cdot N} + R^{|j|}}} \tag{60}$$

which for the pulse-to-pulse jitter simplifies to

$$\rho_{A,J}^{\mathrm{FPF}} = \sqrt{\frac{2}{\frac{1+R}{1-R} + \frac{1+R^N}{1-R^N}}}. \tag{61}$$

Equation (61) is plotted versus the FPF finesse and for PRBS orders $n = 3, 7, 11, 31$ in Fig. 4(a). As it can be verified from the figure, the remaining jitter in the clock signal is drastically reduced to 5%–50% of the jitter existing in the incoming data, depending on the FPF finesse.

Jitter reduction is also possible when the jitter bandwidth is comparable to the FPF FSR, however in this case the jitter rms deviation ratios of (60) have to be calculated for a given jitter spectral power density. Fig. 4(b) plots the results of the calculation for the FPF-based clock recovery, when the jitter spectral power density is Gaussian, as in (46). Fig. 4(b) shows that both the amplitude and the timing jitter can be drastically reduced to 30%, however higher FPF finesse values are required as compared to the pulse-to-pulse jitter case of Fig. 4(a).

In the extreme case where the jitter bandwidth is small compared to the interferometer FSR, similar to the correlated jitter regime of the rate multiplication case, then the autocorrelation function is practically unity for all τ, and (60) reduces to

$$\rho_{A,J}^{\mathrm{FPF}} \cong 1. \tag{62}$$

This is clearly shown in Fig. 4(c), where there is only a marginal reduction in the jitter of the clock signal at the output of the FPF. This marginal reduction is also expected for any type of interferometer, since (62) generally holds, as it can be easily shown after setting the jitter autocorrelation function equal to unity in (58).

V. Conclusion

In this paper, we discussed the impact of passive optical interferometers on the additive noise, the amplitude jitter and timing jitter of the input signals by associating theoretically the input and output noise and jitter in terms of the autocorrelation functions of the input signal, the interferometer impulse response and the noise and jitter. We applied the results of the theoretical analysis to evaluate the performance of interferometer-based rate multiplication and clock recovery schemes, showing that it is possible to reduce additive noise and amplitude jitter when employing interferometers in rate multiplication configurations, although the timing jitter may be aggravated by the multiplication factor unless certain conditions are met. Moreover, we discussed the deployment of FPFs in rate multipliers and provided guidelines for selecting their finesse so as to meet certain quality requirements for the produced high-rate pulse train in terms of its noise and jitter. As far as the interferometer-based clock recoveries are concerned, we showed that both noise and jitter are always reduced, irrespective of the interferometer characteristics. The FPF-based clock recovery, in particular, is capable of reducing amplitude and timing jitter up to 5%–30%, depending on its finesse and the jitter bandwidth, and is a perfectly suitable candidate to deploy in regeneration schemes. We believe that this work can be of practical importance for accurately estimating the jitter at the output of interferometer-based systems when they operate at rates over 100 Gb/s where no testing equipment exists, and as a design tool for determining the interferometer impulse response in order to achieve optimal noise and jitter at its output.

References

[1] K. Yiannopoulos, K. Vyrsokinos, D. Tsiokos, E. Kehayas, N. Pleros, G. Theophilopoulos, T. Houbavlis, G. Guekos, and H. Avramopoulos, "Pulse repetition frequency multiplication with spectral selection in Fabry–Pérot filters," *IEEE J. Quantum Electron.*, vol. 40, no. 2, pp. 157–165, Feb. 2004.

[2] R. Slavik and S. LaRochelle, "Design of 10-to-40 GHz and higher pulse-rate multiplication by means of coupled Fabry–Pérot resonators," *Opt. Commun.*, vol. 247, no. 4–6, pp. 307–312, Mar. 15, 2005.

[3] D. K. Serkland, G. D. Bartolini, W. L. Kath, P. Kumar, and A. V. Sahakian, "Rate multiplication of a 59-GHz soliton source at 1550 nm," *J. Lightw. Technol.*, vol. 16, no. 4, pp. 670–677, Apr. 1998.

[4] T. Sizer, "Increase in laser repetition rate by spectral selection," *IEEE J. Quantum Electron.*, vol. 25, no. 1, pp. 97–103, Jan. 1989.

[5] J. Azana, R. Slavik, P. Kockaert, L. R. Chen, and S. LaRochelle, "Generation of customized ultrahigh repetition rate pulse sequences using superimposed fiber Bragg gratings," *J. Lightw. Technol.*, vol. 21, no. 6, pp. 1490–1498, Jun. 2003.

[6] J. Magne, S. LaRochelle, and L. R. Chen, "50 to 350 GHz pulse bursts generation," in *Proc. Quantum Electron. Laser Science Conf. 2005*, May 2005, vol. 2, pp. 1304–1306.

[7] T. J. Eom, S.-J. Kim, T.-Y. Kim, C.-S. Park, U.-C. Paek, and B. H. Lee, "Realization of true-time-delay using cascaded long-period fiber gratings: theory and applications to the optical pulse multiplication and temporal encoder/decoder," *J. Lightw. Technol.*, vol. 23, no. 2, pp. 597–608, Feb. 2005.

[8] G. E. Town, K. Chan, and G. Yoffe, "Design and performance of high-speed optical pulse-code generators using optical fiber Bragg gratings," *IEEE J. Sel. Top. Quantum Electron.*, vol. 5, no. 5, pp. 1325–1331, Sep./Oct. 1999.

[9] E. Kehayas, L. Stampoulidis, H. Avramopoulos, Y. Liu, E. Tangdiongga, and H. Dorren, "40 Gb/s all-optical packet clock recovery with ultrafast lock-in time and low inter-packet guardbands," *Opt. Exp.*, vol. 13, no. 2, pp. 475–480, Jan. 24, 2005.

[10] G. Contestabile, A. D'Errico, M. Presi, and E. Ciaramella, "40-GHz all-optical clock extraction using a semiconductor-assisted Fabry–Pérot filter," *IEEE Photon. Technol. Lett.*, vol. 16, no. 11, pp. 2523–2525, Nov. 2004.

[11] T. Wang, C. Lou, L. Huo, Z. Wang, and Y. Gao, "Combination of comb-like filter and SOA for preprocessing to reduce the patten effect in the clock recovery," *IEEE Photon. Technol. Lett.*, vol. 16, no. 2, pp. 614–616, Feb. 2004.

[12] C. Bintjas, K. Yiannopoulos, N. Pleros, G. Theophilopoulos, M. Kalyvas, H. Avramopoulos, and G. Guekos, "Clock recovery circuit for optical packets," *IEEE Photon. Technol. Lett.*, vol. 14, no. 9, pp. 1363–1365, Sep. 2002.

[13] M. Jinno and T. Matsutomo, "Optical tank circuits used for all-optical timing recovery," *IEEE J. Quantum Electron.*, vol. 28, no. 4, pp. 895–900, Apr. 1992.

[14] G. T. Kanellos, L. Stampoulidis, N. Pleros, T. Houbavlis, D. Tsiokos, E. Kehayas, H. Avramopoulos, and G. Guekos, "Clock and data recovery circuit for 10-Gb/s asynchronous optical packets," *IEEE Photon. Technol. Lett.*, vol. 13, no. 11, pp. 1666–1668, Nov. 2003.

[15] D. von der Linde, "Characterization of the noise in continuously operating mode-locked lasers," *Appl. Phys. B*, vol. 39, no. 4, pp. 201–217, Apr. 1986.

[16] U. Keller, K. D. Li, M. Rodwell, and D. M. Bloom, "Noise characterization of femtosecond fiber Raman soliton lasers," *IEEE J. Quantum Electron.*, vol. 25, no. 3, pp. 280–288, Mar. 1989.

[17] R. Paschotta, B. Rudin, A. Schlatter, G. J. Spuhler, L. Krainer, S. C. Zeller, N. Haverkamp, H. R. Telle, and U. Keller, "Relative timing jitter measurements with an indirect phase comparison method," *Appl. Phys. B.*, vol. 80, no. 2, pp. 185–192, Feb. 2005.

[18] H. Tsuchida, "Timing-jitter measurement of 78-GHz optical time-division multiplexed pulses by optoelectronic harmonic mixing," *Opt. Lett.*, vol. 27, no. 22, pp. 2040–2042, Nov. 15, 2002.

[19] L. A. Jiang, S. T. Wong, M. E. Grein, E. P. Ippen, and H. A. Haus, "Measuring timing jitter with optical cross correlations," *IEEE J. Quantum Electron.*, vol. 38, no. 8, pp. 1047–1052, Aug. 2002.

[20] M. C. Gross, M. Hanna, K. M. Patel, and S. E. Ralph, "Spectral method for the simultaneous determination of uncorrelated and correlated amplitude and timing jitter," *Appl. Phys. Lett.*, vol. 80, no. 20, pp. 3694–3696, May 20, 2002.

[21] M. Jinno, "Correlated and uncorrelated timing jitter in gain-switched laser diodes," *IEEE Photon. Technol. Lett.*, vol. 5, no. 10, pp. 1140–1143, Oct. 1993.

[22] J. G. Proakis, *Digital Communications*, 4th ed. New York: McGraw-Hill, 2001.

[23] M. H. Hayes, *Statistical Digital Signal Processing and Modeling*, 1st ed. New York: Wiley, 1997.

[24] M. Menif, W. Mathlouthi, P. Lemieux, L. A. Rusch, and M. Roy, "Error-free transmission for incoherent broadband optical communications systems using incoherent-to-coherent wavelength conversion," *J. Lightw. Technol.*, vol. 23, no. 1, pp. 287–294, Jan. 2005.

[25] Z. Zhu, M. Funabashi, Z. Pan, L. Paraschis, and S. J. B. Yoo, "10000-Hop cascaded in-line all-optical 3R regeneration to achieve 1250000-km 10-Gb/s transmission," *IEEE Photon. Technol. Lett.*, vol. 18, no. 5, pp. 718–720, Mar. 1, 2006.

[26] F. Rana, H. L. T. Lee, R. J. Ram, M. E. Grein, L. A. Jiang, E. P. Ippen, and H. A. Haus, "Characterization of the noise and correlations in harmonically mode-locked lasers," *J. Opt. Soc. Amer. B*, vol. 19, no. 11, pp. 2609–2621, Nov. 2002.

[27] O. Leclerc, B. Lavigne, E. Balmefrezol, P. Brindel, L. Pierre, D. Rouvillain, and F. Seguineau, "Optical regeneration at 40 Gb/s and beyond," *J. Lightw. Technol.*, vol. 21, no. 11, pp. 2779–2790, Nov. 2003.

[28] C. Bintjas, N. Pleros, K. Yiannopoulos, G. Theophilopoulos, M. Kalyvas, H. Avramopoulos, and G. Guekos, "All-optical packet address and payload separation," *IEEE Photon. Technol. Lett.*, vol. 14, no. 12, pp. 1728–1730, Dec. 2002.

[29] X. Zhou, C. Lu, P. Shum, H. H. M. Shalaby, T. H. Cheng, and P. Ye, "A performance analysis of an all-optical clock extraction circuit based on Fabry–Perot filter," *J. Lightw. Technol.*, vol. 19, no. 5, pp. 603–613, May 2001.

[30] S. W. Golomb, *Shift Register Sequences*, rev. ed. Walnut Creek, CA: Aegean Park.

Konstantinos Yiannopoulos was born in Tripoli, Greece, in December 1977. He received the Diploma and Ph.D. degrees in electrical and computer engineering from the National Technical University of Athens, Athens, Greece, in 2000 and 2004, respectively.

He is currently a Postdoctoral Researcher at the Computer Engineering and Informatics Department, University of Patras, Patras, Greece. He was with the Photonics Communications Research Laboratory, National Technical University of Athens, from 1999 to 2004. His research related experience includes all-optical high-speed logic, optical signal processing for packet and burst switched networks, and high-rate optical sources. He is the author or coauthor of more than ten papers in IEEE journals and sponsored conferences.

Dr. Yiannopoulos is a member of the IEEE Lasers and Electro-Optics Society (LEOS) and the IEEE Communications Society. He is also one of the recipients of the IEEE LEOS Graduate Student Fellowship Award 2004.

George Theodore Kanellos graduated in 2002 with specialization in telecommunications from the Department of Electrical and Computer Engineering, National Technical University of Athens, Athens, Greece, where he is currently working toward the Ph.D. degree in the Photonics Communications Research Laboratory.

His interests focus on all-optical processing, mainly in the design and implementation of large-scale optical subsystems for TDM/WDM optical networks. He has investigated several techniques for regeneration, clock recovery, burst mode reception and optical logic circuits by exploiting the nonlinear effects of semiconductor optical amplifiers in optical interferometers. His research also concerned the theoretical investigation and development of filtering techniques, using Fabry–Pérot filters and ring resonators, with application in the field of RF-photonics.

Mr. Kanellos is a student member of IEEE Lasers and Electro-Optics Society and a member of the Technical Chamber of Greece.

Nikos Pleros was born in Athens, Greece, in September 1976. He received the Diploma of Electrical and Computer Engineering and the Ph.D. degree in electrical and computer engineering from the National Technical University of Athens (NTUA), Athens, Greece, in 2000 and 2004, respectively.

He is currently continuing research as a Research Associate in the Photonics Communications Research Laboratory, NTUA. His research interests include continuous-wave and mode-locked laser sources for high data-rate telecommunication applications, all-optical digital logic modules, all-optical signal processing, all-optical packet/burst switching and semiconductor-based switching devices.

Dr. Pleros has been awarded the 15th prize in the Greek Mathematical Olympiad in 1993 and was also one of the 12 recipients worldwide of the IEEE/Lasers and Electro-Optics Society (LEOS) Graduate Student Fellowship Award 2003. He is a member of the IEEE LEOS society, the IEEE Communication Society, the Optical Society of America, and of the Greek Technical Chamber.

Hercules Avramopoulos received the Ph.D. degree from Imperial College London, London, U.K.

He is currently heading the Photonics Communications Research Laboratory of the National Technical University of Athens (NTUA), Athens, Greece. From 1989 to 1993, he worked for AT&T Bell Laboratories, Holmdel, NJ. His primary research interest is in the demonstration and application of novel concepts in photonic technologies for telecommunications. He has worked on pulse generation, amplification, and transmission in optical fibers as well as on a large number of laser and amplifier systems for a variety of applications. For the past 15 years, he has been working on ultrahigh-speed, bitwise, all-optical, logic circuits and he has been interested to demonstrate their feasibility as a commercially viable technology for the telecommunications industry. He has been awarded four international patents in ultrahigh-speed switching systems and has more than 100 archival journal publications and presentations in the major international conferences of the field.